ARTICLES

Orbital Interaction Mechanisms of Conductance Enhancement and Rectification by Dithiocarboxylate Anchoring Group

Zhenyu Li and Daniel S. Kosov*

Department of Chemistry and Biochemistry, University of Maryland, College Park, Maryland 20742

Received: August 8, 2006

We study computationally the electron transport properties of dithiocarboxylate terminated molecular junctions. Transport properties are computed self-consistently within density functional theory and nonequilibrium Green's functions formalism. A microscopic origin of the experimentally observed current amplification by dithiocarboxylate anchoring groups is established. For the 4,4′-biphenyl bis(dithiocarboxylate) junction, we find that the interaction of the lowest unoccupied molecular orbital (LUMO) of the dithiocarboxylate anchoring group with LUMO and highest occupied molecular orbital (HOMO) of the biphenyl part results in bonding and antibonding resonances in the transmission spectrum in the vicinity of the electrode Fermi energy. A new microscopic mechanism of rectification is predicted based on the electronic structure of asymmetrical anchoring groups. We show that the peaks in the transmission spectra of 4′-thiolato-biphenyl-4-dithiocarboxylate junction respond differently to the applied voltage. Depending upon the origin of a transmission resonance in the orbital interaction picture, its energy can be shifted along with the chemical potential of the electrode to which the molecule is more strongly or more weakly coupled.

I. Introduction

One of the main goals in nanotechnology is the construction, measurement, and modeling of electronic circuits in which molecular systems act as conducting elements.[1,2] When a molecule is attached to two macroscopic metal electrodes with different chemical potentials, the electric current flows through it. The coupling to electrodes mixes the discrete molecular levels with the continuum of the metal electronic states such that the molecular orbitals protrude deep inside the electrode. The coupling also renormalizes the energies of the molecular orbitals. Therefore, it is no longer correct to talk about the transport properties of the molecule, but rather, only of the electrode−molecule−electrode heterojunction. If the strength of the molecule−electrode coupling is large, then substantial perturbation of the molecular electronic structure can occur. In fact, upon initial chemisorption, it is expected that substantial charge transfer takes place between the metal electrode and the molecule even in the absence of an applied voltage bias. These effects are pivotal for molecular wire transport properties, and they can be controlled by changing the interface geometry or by altering the anchoring groups, which provide the linkage between the molecule and the electrode.[3−10] Therefore, the study of the anchoring group chemistry in molecular electronics may help us not only to pin down the origin of significant discrepancy between experimental and theoretical molecular conductivities but may also reveal new fascinating fundamental aspects of molecule−surface interactions. With only a few exceptions,[11−13] the most widely used molecular wire junctions have been formed so far by organic molecules that are assembled between gold electrodes via thiol anchoring groups. However, thiol linkage is considered to be only structural and lacks any subsequent useful "chemistry",[12] because the energy and the electron occupation of the sulfur 3p orbital are difficult to modify. Tulevski et al.[12] thus suggested to use a ruthenium rather than a gold electrode. But because gold is an excellent conductor and a metal with mature manipulation techniques, gold remains the most attractive electrode material.

The quest for reliable molecular electronic devices has become the search for better molecule−gold linkers,[14] which provide the opportunity not only to grow the single molecular contacts but also to control molecular transport properties. Recently, Tivanski et al.[15] suggested and realized experimentally the remarkable molecular wire, which is attached to the gold electrodes via dithiocarboxylate conjugated linker ($-CS_2$). The conductance of 4,4′-biphenyl dithiolate (BDT) and 4,4′-biphenyl bis(dithiocarboxylate) (BDCT) molecular wires were measured by conducting-probe atomic force microscopy.[15] The central conducting parts of both BDT and BDCT are exactly the same (biphenyl), whereas the anchoring groups are different. BDT has the standard thiol groups, and BDCT is terminated by dithiocarboxylate groups. It was experimentally observed that the conductance of BDCT is 1.4 times as large as the conductance of BDT.[15] But the physical origin of this conductance enhancement was not clear. The most intuitive picture suggests that the conjugated dithiocarboxylate anchoring group provides the stronger coupling between the electrode and the molecule.[15] We recently have demonstrated that this simple mechanism plays a central role in conductance enhancement induced by the dithiocarbomate linker ($N-CS_2$)[10] in which the stronger molecule−electrode coupling leads to the larger mixing

* Corresponding author. Email: dkosov@umd.edu.

10.1021/jp065120t CCC: $33.50
Published on Web 09/14/2006

between the discrete molecular levels and the continuum of the metal electronic states and, thus, to the larger broadening of resonances in the electron transmission spectrum. As it turned out, the mechanism of the conductance enhancement is entirely different for dithiocarbamate and dithiocarboxylate linkers, although they are structurally very similar. One of the aims of this paper is to elucidate the microscopic origin of the conductance enhancement via dithiocarboxylate linkers. We show that the reason for the conductance enhancement is not simply the difference in the molecule−electrode coupling strengths but is also the disparity in the electronic structure of thiol and dithiocarboxylate anchoring groups.

One of the interesting possibilities is the use of dithiocarboxylate linkers to create a molecular rectifier. A molecular rectifier is a junction in which electrons flow along one preferential direction.[16,17] As a prototype molecular junction, we consider biphenyl with a thiol linker on one side and with a dithiocarboxylate anchoring group on the other: 4′-thiolato-biphenyl-4-dithiocarboxylate (TBCT). Rectification for molecules with asymmetric anchoring groups has been studied theoretically.[10,18] However, in all junctions considered so far, the role of anchoring groups was limited to providing left−right asymmetry in the coupling strength between the molecule and the electrodes. It leads to the standard coupling-strength picture of molecular rectification, which predicts that as the voltage bias increases, the peaks in the transmission are shifted along with the chemical potential of the electrode to which the molecule is more strongly coupled.[10,18] Suppose, for example, that there are two resonances in the transmission spectrum in the vicinity of the electrode Fermi energy with the energies above and below it so that both resonances contribute to the electron transport at moderate voltages. Within the standard rectification picture, the two peaks are shifted in the same direction.[10,18] Therefore, when the energy of one resonance enters the integration range between the chemical potentials of the left and the right electrodes (i.e., it starts to contribute to the electron current), the second resonance already could be shifted away from the integration range. Thus, as soon as the contribution from one peak to the current increases, the role of the second peak decreases. This counterbalancing reduces the rectification effects within the standard coupling-strength mechanism. In this paper, we show that the TBCT molecular junction exhibits an entirely new mechanism of rectification, which overcomes the limitations of the standard coupling-strength picture described above.

The remainder of the paper is organized as follows. In section II, we describe the computational details. The main results are discussed in section III. We first illustrate how the electronic structure of thiol and dithiocarboxylate anchoring groups control and determine transport properties of molecular wire junctions. A new rectification mechanism is suggested for molecule attached to electrodes by thiol and dithiocarboxylate groups. Section IV concludes the paper.

II. Computational Methods

Two computer programs were used in our calculations. First, optimized geometries of the molecular junctions were obtained by the SIESTA computer program.[19] Then, electron transport properties were computed by using TranSIESTA-C package.[20] TranSIESTA-C uses the combination of nonequilibrium Green's function (NEGF) formalism and density functional theory (DFT). In NEGF theory, the molecular wire junction is divided into three regions: left electrode (L), contact region (C), and right electrode (R). The semi-infinite electrodes are calculated separately to obtain the bulk self-energy. The contact region contains parts of the electrodes to include the screening effects in the calculations. The electrodes are modeled by semi-infinite Au surfaces. The main loop for TranSIESTA-C self-consistent NEGF/DFT calculations is described below (we refer to ref 20 for technical details).[20] The matrix product of the Green's function and the imaginary part of the left/right electrode self-energy yields the spectral densities. The spectral densities of the left and right electrodes are combined together to compute the nonequilibrium, voltage-dependent density matrix, and then the density matrix is converted into nonequilibrium electron density. The nonequilibrium electron density enables us to compute matrix elements of Green's function. The Hartree potential is determined through the solution of the Poisson equation with appropriate voltage-dependent boundary conditions. This loop of calculations is repeated until self-consistency is achieved. After the self-consistent convergence is achieved, the voltage transmission spectrum is calculated by the standard equation

$$T(E, V) = Tr[\Gamma_L(E, V)\mathbf{G}(E, V)\Gamma_R(E, V)\mathbf{G}^{\dagger}(E, V)] \quad (1)$$

where $\mathbf{G}$ is the Green's function of the contact region, $\Gamma_{L/R}$ is the coupling matrix, and V is the applied voltage bias. The electric current as a function of the applied voltage is obtained by the integration of the transmission spectrum

$$I(V) = (-e)\int T(E, V)(f(E - \mu_L) - f(E - \mu_R))\mathrm{d}E \quad (2)$$

where f is the Fermi−Dirac occupation number, $\mu_L = -eV/2$ ($\mu_R = eV/2$) is the chemical potential for the left (right) electrode, and e is the elementary charge.

We use double-ζ with polarization (DZP) basis for all atoms except Au for which single-ζ with polarization (SZP) is used. We use Troullier−Martins nonlocal pseudopotentials in all our calculations.[21] The exchange-correlation potential is described by Perdew−Zunger local density approximation (LDA).[22] Single k-point sampling on the plane perpendicular to the direction of the current is used in our calculations. Our tests show that the generalized gradient approximation[23] yields negligible corrections to the LDA transmission spectra, and the use of 4×4 k-point sampling does not affect main features of the transmissions.

III. Results and Discussion

A. Structural Model of Molecular Junctions. We consider three representative molecular wire junction systems: BDT, BDCT, and TBCT. BDT and BDCT are terminated by thiol and dithiocarboxylate, respectively, on both ends. In TBCT, a dithiocarboxylate group is used on the left side, while a thiol group is used on the right side. Figure 1 shows the optimized junction geometries. The semi-infinite left and right electrodes are modeled by two Au(111)−(3×3) surfaces for which only one unit cell which contains three Au layers, is plotted. In the contact region, two Au layers at both left and right side are included. The outmost left and right layers in the contact regions are constrained to their theoretical bulk geometry to match the structure of Au(111)−(3×3) surfaces, which are used to model the electrodes. We assume the biphenyl interior part of all three junctions have coplanar geometry. This narrows down the problem of difference between BDT, BDCT, and TBCT transport properties to the role of the dithiocarboxylate linkers. The rest of the contact region is fully optimized. We also optimized the length of the junctions by computing the total

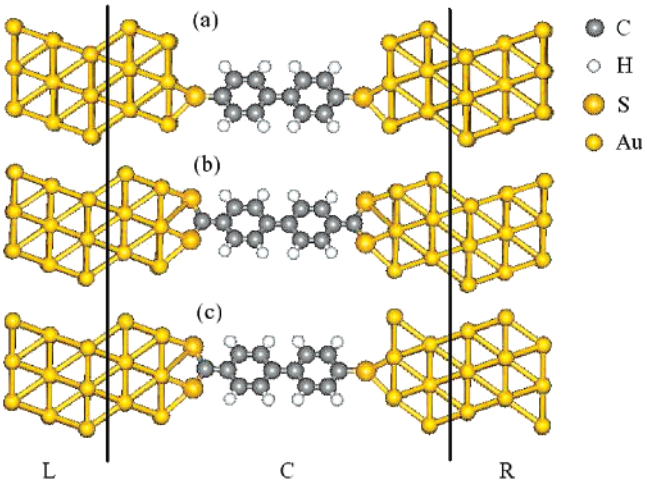

Figure 1. Relaxed geometry of molecular wire junctions with different anchoring groups. (a) BDT, (b) BDCT, (c) TBCT. Only one unit cell for the semi-infinite electrode is plotted.

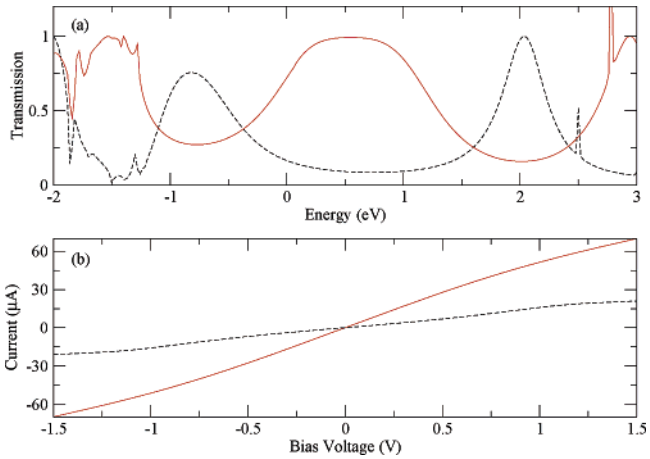

Figure 2. (a) Zero voltage bias transmission spectra and (b) current−voltage characters of BDT (dashed) and BDCT (solid) molecular junctions. Fermi energy of the electrode is set to zero in the transmission spectra.

energies of the systems as functions of the distance between the left and the right electrodes. Every single energy point is calculated by performing geometry optimization with constrained electrode−electrode separation. The optimal separation between the electrodes is obtained as the distance at which the total energy is minimal. We also perform test calculations for noncoplanar BDT and BDCT. The twisting of phenyl rings by 37°, which corresponds to the equilibrium geometry for biphenyl junction,[6] has negligible influence on the transmission spectra. The twisting merely reduces the overall transmission probability without any further alternation of the transmission spectra.

B. Orbital Interaction Mechanism of Conductance Enhancement. With the optimized geometries, we calculate transmission spectra and current−voltage ($I-V$) characteristics for BDT and BDCT as shown in Figure 2. The computed current is 4 orders of magnitude larger than the experimental one.[15] Our $I-V$ curves qualitatively reproduce the experimental conductance enhancement, although the theoretically predicted increase in conductivity (∼2.1) is larger than the experimentally observed amplification factor (∼1.4).[15] The conductance enhancement is shown clearly in the transmission spectra. For BDT, there are two broad peaks: one is below the electrode Fermi energy (∼ −0.8 eV), and the other is above it (∼2.1 eV). These two peaks still can be found in the transmission spectrum of BDCT, but the first peak is shifted toward the lower

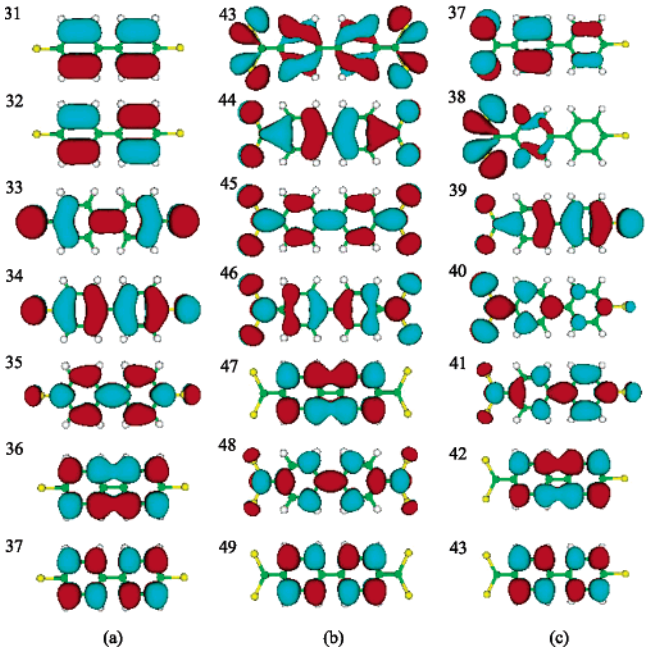

Figure 3. MPSH orbitals near gold electrode Fermi level for (a) BDT, (b) BDCT, and (c) TBCT.

TABLE 1: Energies of Molecular Orbitals of Biphenyl and MPSH Orbitals of BDT, BDCT, and TBDT[a]

biphenyl		BDT		BDCT		TBDT	
n	ϵ_n (eV)	n	ϵ_n (eV)	n	ϵ_n (eV)	n	ϵ_n (eV)
25	−3.926	31	−2.580	43	−2.222	37	−2.343
26	−3.201	32	−2.433	44	−1.821	38	−2.230
27	−3.052	33	−2.341	45	0.003	39	−1.489
28	−2.358	34	−1.271	46	0.849	40	0.433
29	1.229	35	1.838	47	2.772	41	2.305
30	1.840	36	2.506	48	2.808	42	2.559
31	2.350	37	3.020	49	3.257	43	3.087

[a] All energies are relative to the Fermi energy of the gold electrode.

energy (∼ −1.5 eV) and the second peak is moved to the higher energy (∼2.9 eV). Besides these two peaks, the additional broad peak appears for BDCT just above the Fermi energy. It gives almost perfect transmission probability in the broad energy range from 0.1 to 1.1 eV. This broad peak results in large transmission probability at the Fermi energy and is responsible for the conductance enhancement for the BDCT junction observed on experiment.[15]

The microscopic origin of this broad peak and, thus, the cause of the conductance enhancement can be understood from the partitioning of the transport channels into contribution from the interior part (biphenyl) and the linkers (thiol or dithiocarboxylate). If we project the self-consistent Hamiltonian onto the Hilbert space spanned by the basis functions of the molecule (includes biphenyl and anchoring groups), we obtain the molecular projected self-consistent Hamiltonian (MPSH). The eigenstates of MPSH can be considered as molecular orbitals renormalized by the molecule−electrode interaction. Figure 3 shows the MPSH orbitals near the Fermi level of the electrodes and Table 1 shows the corresponding eigenvalues. When the energies of the resonances in the transmission spectra are compared with the eigenvalues of MPSH, we find that the two main transmission peaks of BDT mainly are contributed by MPSH orbitals 34 and 35, while the peaks of BDCT take their origin from MPSH orbitals 44, 45, 46, and 48. The common feature of these orbitals is the significant delocalization and spread of the electron density along the interior region of the

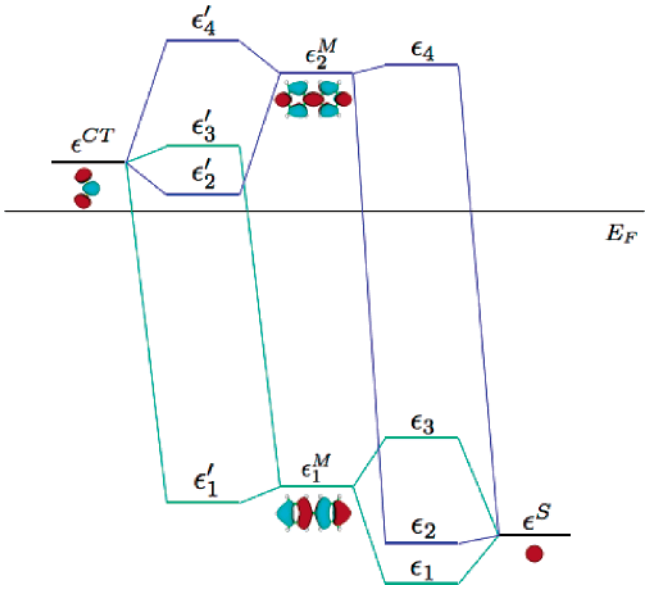

Figure 4. Schematic orbital interaction picture. Interaction between biphenyl HOMO/LUMO and anchoring group orbitals (sulfur p and dithiocarboxylate LUMO) leads to MPSH orbitals.

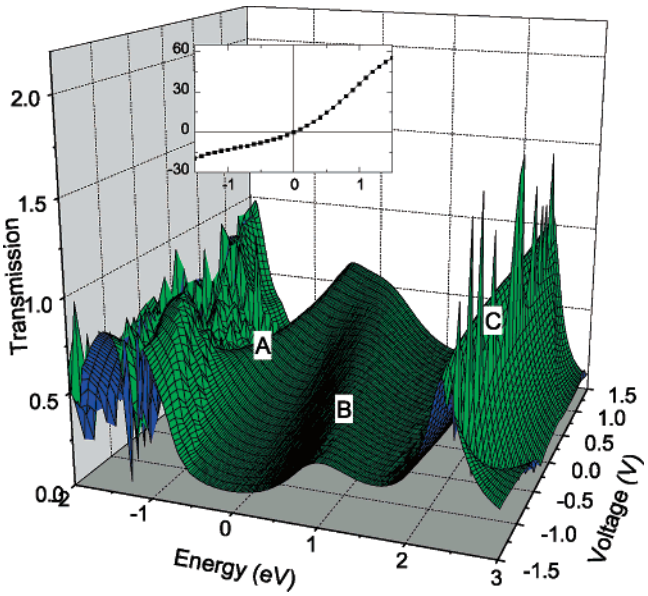

Figure 5. Voltage-dependent transmission spectrum of the TBCT junction. Inset: current−voltage curve with voltage (in V) as the abscissa and current (in μA) as the ordinate.

wire as well as the anchoring groups. The additional peak in the transmission spectrum of BDCT is not a single broad resonance. As indicated by the MPSH analysis, the merging of two resonances from MPSH orbitals 45 and 46 produces this broad peak. Peaks in BDTC transmission do not show significant additional broadening with respect to BDT resonances.

The MPSH orbitals can be further disentangled if we consider them as generated by the interaction between orbitals localized on the anchoring groups and orbitals of the interior part (biphenyl molecule). When all relevant MPSH orbitals for the three junctions are dissected, it is shown that all of them can be obtained from linear combinations of the two anchoring group orbitals (sulfur 3p orbital of thiol linkage and lowest unoccupied molecular orbital (LUMO) of dithiocarboxylate) and the highest occupied molecular orbital (HOMO)/LUMO of the biphenyl molecule. This orbital interaction picture is presented in Figure 4. The biphenyl HOMO and LUMO (orbitals 28 and 29, respectively, in Table 1), are labeled as ϵ_1^M and ϵ_2^M, respectively, in Figure 4. The sulfur 3p atomic orbital of thiol linkage (ϵ^S)lies very deep (−2.88 eV from the calculation of atomic energy levels of sulfur) below the Fermi energy of the gold surface.[12] When the thiol group is attached to biphenyl, the resultant MPSH orbitals are all far from the Fermi level, and only the antibonding orbitals (ϵ_3 and ϵ_4) contribute to low-voltage electron transport. From Figure 3a, we can easily identify ϵ_3 and ϵ_4 as BDT MPSH orbitals 34 and 35, respectively.

The orbital interaction picture leads to a very different mechanism of electron transport through BDCT molecular wire. Here, orbital interaction between the LUMO of the dithiocarboxylate group (ϵ^{CT}) and the biphenyl HOMO/LUMO contributes to the four resonance structures in the transmission spectrum. The value of ϵ^{CT} (0.35 eV from the calculation of H_2S_2−CH molecular orbitals) is much higher than ϵ^S in the thiol, and therefore, both bonding and antibonding MPSH orbitals of BDCT are positioned in the vicinity of the Fermi energy and contribute to low bias electron transport. The right side of Figure 4 shows the orbital interaction picture for BDCT in which levels ϵ_1'−ϵ_4' correspond to MPSH orbitals 44, 45, 46, and 48, respectively. Level ϵ_2', which is almost in resonance with the electrode Fermi energy, gives the main contribution to low-voltage electron transport. Therefore, it is the intrinsic electronic structure difference between the anchoring groups that is the real origin for the observed conductance enhancement by the dithiocarboxylate anchoring group.

TABLE 2: Energies (in eV) of the Peaks A, B, and C from Figure 5 for Different Values of the Applied Voltage (in V)

voltage	A	B	C
1.5	−0.4	0.0	2.4
0.5	−0.7	0.3	2.4
0.0	−0.9	0.5	2.4
−0.5	−1.3	0.7	2.4
−1.5	−1.5	1.0	2.4

C. Rectification. In this section, we demonstrate that TBCT exhibits a new mechanism of rectification. The new mechanism enables us to overcome the limitation of the standard coupling-strength picture[10,18] in which rectification from one resonance could be reduced by the opposite contribution from another resonance.

The voltage dependence of the transmission spectrum of TBCT junction shows very complicated patterns (Figure 5 and Table 2). There are three main transmission peaks. The left peak (A) shifts toward the higher energy as the voltage changes from negative to positive bias, the middle peak (B) shows the opposite behavior, and the right peak (C) does not shift at all. This means that peak A follows the changes in the chemical potential of the right electrode ($\mu_R = eV/2$), while peak B follows the chemical potential of the left electrode ($\mu_L = -eV/2$). The $I-V$ curve is shown in the inset of Figure 5. It is obtained by integrating the transmission from μ_L to μ_R. For negative bias voltage, both peaks A and B are not within the integration range, and, therefore, the current is small. Under positive voltage, when the value of the voltage increases, both A and B enter the integration region and produce a large current increase. Thus, we obtain rectification coefficient $R = I(V)/I(-V) \sim 2.8$ at 1.0 eV bias voltage.

The response of the transmission spectrum on the applied voltage bias can be readily understood if we look at the MPSH orbitals as plotted in Figure 3c. Peaks A, B, and C correspond to MPSH orbitals 39, 40, and 41, respectively. Orbital 39 has stronger molecule−electrode coupling via the thiol group, so that the energy of this orbital follows the chemical potential of

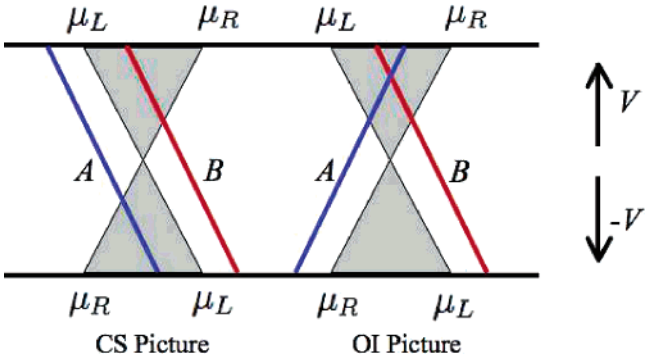

Figure 6. Coupling strength (CS) and orbital interaction (OI) mechanisms for current rectification. The transmission from the shadow region contributes to current (see eq 2). Blue and red lines represent two transmission resonances A and B.

the right electrode. This orbital is mainly an antibonding mixture of the HOMO of biphenyl (ϵ_1^M in Figure 4) and the 3p orbital of the sulfur (ϵ^S). Therefore, orbital 39 (ϵ_3 plus minor contribution from ϵ_1') has stronger coupling at the thiol side. Similarly, orbital 40 is mainly related to ϵ_2', which has stronger coupling via the dithiocarboxylate group and follows the chemical potential of the left electrode. Orbital 41 is antibonding at both sides and can be considered a combination of ϵ_4 and ϵ_4'. Orbital 41 interacts equally well with both electrodes. Therefore, the influence of the left electrode is balanced by the influence of the right electrode, and this orbital is not significantly affected by the applied voltage. To summarize, likewise in the case of the conductance enhancement, the electronic structure of the anchoring groups and orbital interaction picture provides the explanation of why these three transmission peaks behave differently under the voltage bias.

The schematic diagram, which shows the qualitative behavior of the two peaks, is shown in Figure 6. In the standard coupling-strength picture, all transmission peaks follow the chemical potential of the stronger-coupled electrode (left electrode in the figure).[10,18] If there are two transmission peaks equally spaced below and above the mean Fermi level of the electrode (A and B in Figure 6), their contributions to the rectification counteract each other. At the negative bias, peak A enters the integration range, which increases the current, compared to that at the positive bias. The current prefers to flow from the right to the left due to peak A. On the other hand, peak B increases the current at positive bias voltage, and, therefore, the current prefers to flow from the left to the right because of peak B. This situation can be avoided in the orbital interaction picture in which peaks A and B respond oppositely on the applied voltage. As shown in the right part of Figure 6, which is exactly the situation we find in the TBCT junction, both peaks A and B rectify the current in the same direction.

IV. Conclusions

We have performed DFT-NEGF calculations to elucidate the microscopic origin of the conductance enhancement via dithiocarboxylate linkers. We showed that the reason for the conductance enhancement was not simply the difference in the molecule−electrode coupling strengths but also in the disparity in the electronic structure of thiol and dithiocarboxylate anchoring groups. We suggested the use of the dithiocarboxylate linker to create a molecular rectifier. As a prototype molecular rectifier, we considered a biphenyl with a thiol linker on one side and with a dithiocarboxylate anchoring group on the other side (TBCT molecule). We predicted that the TBCT molecular junction exhibited an entirely new mechanism of rectification that had never been predicted theoretically or observed experimentally. Our calculations demonstrated how the electronic structure of anchoring groups accompanied by molecular orbital interaction picture can be used as a guiding principle to predict transport properties of molecular junctions.

Acknowledgment. The authors are grateful to M. Gelin, L. Sita, A. Vedernikov, and J. Yang for helpful discussion. This work was partially supported by the American Chemical Society Petroleum Research Fund (44481-G6) and by a summer award of General Research Board of the University of Maryland.

Supporting Information Available: Total energies of the molecular junctions as functions of electrode−electrode separation, transmission spectra for different molecular geometries, transmission spectra computed with GGA exchange-correlation functional, and transmission spectra computed with 4×4 k sampling. This material is available free of charge via the Internet at http://pubs.acs.org.

References and Notes

(1) Nitzan, A.; Ratner, M. A. *Science* **2003**, *300*, 1384.
(2) Joachim, C.; Ratner, M. A. *Proc. Natl. Acad. Sci. U.S.A.* **2005**, *102*, 8801.
(3) Venkataraman, L.; Klare, J. E.; Tam, I. W.; Nuckolls, C.; Hybertsen, M. S.; Steigerwald, M. L. *Nano Lett.* **2006**, *6*, 458.
(4) Li, X.; He, J.; Hihath, J.; Xu, B.; Lindsay, S. M.; Tao, N. *J. Am. Chem. Soc.* **2006**, *128*, 2135.
(5) Kim, B.; Beebe, J. M.; Jun, Y.; Zhu, X.-Y.; Frisbie, C. D. *J. Am. Chem. Soc.* **2006**, *128*, 4970.
(6) Xue, Y.; Ratner, M. A. *Phys. Rev. B* **2003**, *68*, 115406.
(7) Ke, S.-H.; Baranger, H. U.; Yang, W. *J. Am. Chem. Soc.* **2004**, *126*, 15897.
(8) Basch, H.; Cohen, R.; Ratner, M. A. *Nano Lett.* **2005**, *5*, 1668.
(9) Ke, S.-H.; Baranger, H. U.; Yang, W. *J. Chem. Phys.* **2005**, *123*, 114701.
(10) Li, Z.; Kosov, D. S. *J. Phys. Chem. B* **2006**, *110*, 9893.
(11) Siaj, M.; McBreen, P. H. *Science* **2005**, *309*, 588.
(12) Tulevski, G. S.; Myers, M. B.; Hybertsen, M. S.; Steigerwald, M. L.; Nuckolls, C. *Science* **2005**, *309*, 591.
(13) Guo, X.; et al. *Science* **2006**, *311*, 356.
(14) Akkerman, H. B.; Blom, P. W. M.; de Leeuw, D. M.; de Boer B. *Nature* **2006**, *441*, 69.
(15) Tivanski, A. V.; He, Y.; Borguet, E.; Liu, H.; Walker, G. C.; Waldeck, D. H. *J. Phys. Chem. B* **2005**, *109*, 5398.
(16) Aviram, A.; Ratner, M. A. *Chem. Phys. Lett.* **1974**, *29*, 277−283.
(17) Metzger, R. M. *Chem. Rev.* **2003**, *103*, 3803.
(18) Taylor, J.; Brandbyge, M.; Stokbro, K. *Phys. Rev. Lett.* **2002**, *89*, 138301.
(19) Soler, J. M.; Artacho, E.; Gale, J.; Garcia, A.; Junquera, J.; Ordejon, P.; Sanchez-Portal, D. *J. Phys.: Condens. Matter* **2002**, *14*, 2745−2779.
(20) Brandbyge, M.; Mozos, J.-L.; Ordejon, P.; Taylor, J.; Stokbro, K. *Phys. Rev. B* **2002**, *65*, 165401.
(21) Troullier, N.; Martins, J. L. *Phys. Rev. B* **1991**, *43*, 1993.
(22) Perdew, J. P.; Zunger, A. *Phys. Rev. B* **1981**, *23*, 5048.
(23) Perdew, J. P.; Burke, K.; Ernzerhof, M. *Phys. Rev. Lett.* **1996**, *77*, 3865.